

**HYDROCLIMATE MODELING OVER THE HIMALAYAN
BEAS BASIN**

ANKUR DIXIT



**CENTRE FOR ATMOSPHERIC SCIENCES
INDIAN INSTITUTE OF TECHNOLOGY DELHI
AUGUST 2022**

© Indian Institute of Technology Delhi (IITD), New Delhi, 2022

**HYDROCLIMATE MODELING OVER THE HIMALAYAN
BEAS BASIN**

by

ANKUR DIXIT

CENTRE FOR ATMOSPHERIC SCIENCES

Submitted

in fulfilment of the requirements of the degree of Doctor of Philosophy

to the



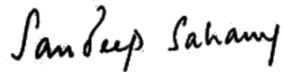
INDIAN INSTITUTE OF TECHNOLOGY DELHI

AUGUST 2022

*To my Parents
And lovely brother
Ashish*

Certificate

This is to certify that the thesis entitled “**Hydroclimate Modeling over the Himalayan Beas Basin**” being submitted by **Mr. Ankur Dixit** to the Indian Institute of Technology Delhi for the award of the degree of **DOCTOR OF PHILOSOPHY** is a record of original bonafide research carried out by him. He worked under my supervision and has fulfilled the requirements for the submission of this thesis. The results contained in this thesis have not been submitted in part or full to any other university or institute for the award of any degree or diploma.



Dr. SANDEEP SAHANY *

Assistant Professor, Centre for Atmospheric Sciences
Indian Institute of Technology Delhi



Dr. SAROJ KANTA MISHRA

YES Foundation Chair for Climate Modeling
Principal Investigator, DST Centre of Excellence in Climate Modeling
Associate Professor, Centre for Atmospheric Sciences
Indian Institute of Technology Delhi

* Now, Head & Deputy Principal Research Scientist, Climate Modeling and Prediction Branch, Centre for Climate Research Singapore

Acknowledgments

I would like to thank my Ph.D. supervisors, Prof. Sandeep Sahany and Prof. Saroj Kanta Mishra, for their support and supervision. I would express my sincere gratitude to Prof. Sandeep Sahany without whom this thesis would never have been possible. His suggestions, timely help, and detailed scientific diagnostics were phenomenal. I am highly thankful to him for his faith, patience, and perseverance with me.

I am thankful to SRC members- Prof. Manju Mohan, Prof. Vimlesh Pant, Prof. Sukumar Mishra, and Head (CAS) Prof. K. AchutaRao for their advices and suggestions. I would like to mention all the administrative staff of CAS office (especially Narendra sir) for all the support.

I want to acknowledge Indian Institute of Technology Delhi (IITD) for providing fellowship and logistic during PhD. I am also grateful to all HPC Team members for all the help and troubleshooting, especially Roshan and Manish.

I would like to thank many people and friends who made this period over IITD pleasant and lively. Thanks to Vivek Singh, Jivesh Dixit, Puneet Sharma, Tanvi, Raju Pathak, Popat Salunke, Asochya, Arora sir, Jyoti Singh, Yajnaseni Dash, Abhishek Anand, Shoobhangi Tyagi, Pankaj, Debi, Prabhakar, Amit, Pawan Vats, Pawan Parmar, Kapil sir for their time over tea breaks and other discussions. Many of them may not have much contribution directly to this thesis but made my life easy and lively. I would like to extend my greatest thanks to my school friends Vikas Mishra (Chimpu) and Harshit Gupta. They were present all the time by my side through all ups and downs, made fun and did counselling, did everything else that was best in my interests. I want to express my thanks to Anant Nautiyal, Mayank Sharma, and Amit Anand for their support and love. Lastly, I would express my thanks to all the people who remained unlisted (friends, family, well-wishers) but have great contributions to shape up this thesis and my life in its present form.

I would like to extend my wholehearted love and affection to dogs (Peepini, PubG, Kalu near canteen, and Nescafe gang) and cats (albert, textile gang, scoop gang) of the campus. They made this journey easy and filled with joy. The bond that I developed with them will remain with me and remind me as one of the golden memories during my stay at IITD.

Ankur Dixit

Abstract

The Himalayan mountains are considered as water towers because of the massive potential of freshwater in glacier ice masses and seasonal snow. They have colossal potential to receive and store the snow during winter and provide fresh water during summer due to snowmelt. Moreover, these mountains have a significant role in regulating global and regional climate. Rapidly rising temperatures caused by global warming could be catastrophic for the people living in this region and downstream as the mountain glaciers are critical for fulfilling the downstream water and energy demand. Therefore, any changes in the climate could implicate widespread impacts on livelihoods as perennial water security and food security are largely dependent on the snow and glacier melt in this region. However, different sub-regions may have different impacts of global warming and, per se, different consequences. Therefore, the planning for adaptation and resilience to the impact of changing climate on water availability require projected estimates based on reliable scenarios.

Hydroclimate modeling over the Beas basin, situated in North-Western Himalayas, is attempted in his study to assess the change in hydrological fluxes under present and future climates. The objective of the thesis is broadly divided into four tasks that start with the sensitivity analysis of Weather Research and Forecasting (WRF) model towards the selected microphysics and cumulus schemes to assess the ability of precipitation simulation over the study region. Next, Glacier model was used to produce the glacier dynamics in the study region under the present and future climates. Next, WRF-Hydro was calibrated using the automatic approach. Lastly, the offline coupled system of WRF and WRF-Hydro was used to produce hydrological fluxes under present and future climates.

Firstly, WRF was set up with three nested domains, the outermost covering the whole Himalayas, the middle covering the whole of the North-West ranges of Himalayas, and the innermost concentrated to the study area. The six experiments with a combination of three microphysics and two cumulus schemes were performed. It was found that the precipitation along the Himalayan foothills (near to basin terminal) is underestimated by four out of six experiments. Only WSM6_BMJ (WSM6 microphysics and BMJ convection scheme) and MP8_BMJ (MP8 microphysics and BMJ convection scheme) were able to show a considerable amount of precipitation along these foothills. However, all six experiments showed high precipitation in the upstream region and the mountain peaks and ridges in North-Western Himalayas. During December-January-February (DJF), MP8_KF, MP3_BMJ, and MP8_BMJ have shown relatively lesser precipitation, however, WSM6_KF and WSM6_BMJ were found to have maximum precipitation. MP8_KF is found to have the least normalized standard deviation, along with a higher skill score than most of the experiments. Overall, MP8_KF could be considered reasonable because of its lesser deviation and better skill score. For June-July-

August-September (JJAS), four (MP3_KF, MP3_BMJ, MP8_KF, WSM6_KF) out of six experiments failed to show the precipitation features in downstream foot-hills at the basin terminal and northern slopes, having average precipitation much lower in comparison to observation. WSM6_BMJ has shown the highest correlation and best skill score, along with the least normalized standard deviation.

Next, The glacier dynamics were simulated and analyzed over the Beas basin (situated in the north-western Himalayas) for the present (1980–2015) and future climates (2006–2100) under RCP4.5 and RCP8.5 global warming scenarios. The Open Global Glacier Model was first calibrated over the study region and then conducted simulations for the present (forced by ERA-Interim) and future (forced by CMIP5 models) climates. For the present climate, the model simulations show that 50% of the total glacier volume (compared to 1980) is lost by 2011, with glacier area and volume showing a significantly decreasing trend, with higher fluctuations in the glacial area during recent decades. Future projections suggest 75% loss by 2040 \pm 2.5 years and \sim 90% loss by 2094 \pm 3.5 years under RCP4.5. Under RCP8.5, 75% loss is expected to occur by 2040 \pm 3 years and \sim 90% by 2084 \pm 8 years. Ensemble mean of the near-surface air temperature (both monthly mean and annual mean) shows a significantly increasing trend under RCP4.5 and RCP8.5 for the entire 21st century. Ensemble mean of the total monthly precipitation shows no trend under RCP4.5, however, it shows a decreasing trend for months OJFMA and an increasing trend for months JJ under RCP8.5. An increase in JJ precipitation does not increase glacier mass since this region does not receive snowfall during these months. Under RCP4.5, snowfall does not show any significant trend during NDJF, however, it shows a decreasing trend during October and March. Under RCP8.5, snowfall shows a significant decreasing trend for October through March. Overall, a similar melting rates were found under RCP4.5 and RCP8.5 until \sim 2050, but the latter shows a higher rate afterward.

Next, the WRF-Hydro calibration was performed using the WRF downscaled meteorological forcing. The model was calibrated for 2003 and validated for 2004-2005. The station observed discharge at the basin outlet was used to perform the calibration and validation. The selected 42 parameters were tuned using PEST (Parameter ESTimation) tool through the model inversion process. The eight simulations were designed using two sets of meteorological forcing (MP8KF forcing and WSM6BMJ forcing). It is found that model calibration improved the accuracy to reproduce the basin discharge. Despite improvement, JJAS discharge was underestimated in MP8KF experiments, possibly due to underestimation in the JJAS precipitation in MP8KF forcing. WSM6BMJ experiments did reasonably well for the JJAS, but it showed some erroneous high peaks for the non-JJAS. These peaks were probably introduced due to the overestimation of the precipitation (for non-JJAS) in WSM6BMJ forcing. Further, the best candidate out of these simulations was picked up, each for MP8KF and WSM6BMJ experiments. Then, the ensemble mean and weighted ensemble of the basin discharge was calculated from these best candidates. The ensemble mean discharge was found

reasonably well for the calibration period (NSE=0.64), however, the accuracy decreases for the validation period. The weighted ensemble of these simulations produces satisfactory results (NSE=0.5), alongside the accuracy increases for the validation period (NSE=0.6).

Next, the WRF with WRF-Hydro was coupled in offline mode. The convection permitting simulations were performed using the WRF model for high-resolution atmospheric forcing (for one historical time slice and three-time slices for future projections under RCP4.5 and RCP8.5). These atmospheric forcing were fed to the hydrological model (WRF-Hydro) to generate high-resolution hydrological fluxes. The updated glacier boundaries were obtained from the glacier model and subsequently ingested to the WRF and WRF-Hydro to represent an updated Land Use Land Cover (LULC). It was found that the total amount of precipitation over the basin does not change by large values in the basin, however, there is a significant contrast in the change of the precipitation pattern. The higher peaks and ridges of the basin are expected to experience lesser precipitation under both RCP4.5 and RCP8.5, having the largest decline for the end of 21st century under RCP8.5. In contrast to this, the downstream regions may get wetter in comparison to the historical time period. The contrast was found mostly because of the composite of the different responses during different seasons (DJF and JJAS). The near-surface air temperature is expected to rise throughout the annual cycle under RCP4.5 and RCP8.5 scenarios. Though RCP4.5 tends to stabilize post-2050, RCP8.5 continues to rise, leading to the significant difference between the temperature of these two scenarios post-2050. The study region is expected to become warmer by 1-3 °C under RCP4.5 and 3-4 °C under RCP8.5 for JJAS at the end of the 21st century. DJF is expected to become warmer by 2.5-3.5 °C under RCP4.5 and 4.5-5 °C under RCP8.5 at the end of this century. The surface runoff is expected to decrease almost throughout the basin. However, it was found to be increased over high peaks during early-21st-century under RCP4.5 and during mid-21st-century under RCP8.5. The largest decline was found at the end of this century under both RCP4.5 and RCP8.5 for higher altitude regions. The subsurface flow (UGDRNOFF) decreased consistently under both RCP4.5 and RCP8.5, with a stronger declining signal under RCP8.5. UGDRNOFF is expected to decrease by ~60% under RCP4.5 and ~70% under RCP8.5 at the end of this century. Under RCP4.5, the snow water equivalent (SNEQV) was found to be decreased for the regions having altitude lower than 5 km, however, the same is found to be increased for the higher elevated regions. A similar response is expected under RCP8.5 until the mid of 21st century, however, towards the end of the century, SNEQV is expected to decline throughout the year across the region. The highest decline in SNEQV could occur during the end of the 21st century for both RCP4.5 and RCP8.5 scenarios. The contrasting response of SNEQV under both scenarios at the end of this century could be because of the different levels of warming.

सारांश

हिमालय के पहाड़ों को जल मीनार के रूप में माना जाता है क्योंकि हिमनदों और मौसमी बर्फ में मीठे पानी की विशाल क्षमता होती है। उनके पास सर्दियों के दौरान बर्फ को संग्रहीत करने और गर्मियों के दौरान बर्फ पिघलने के कारण ताजा पानी उपलब्ध कराने की अत्यधिक क्षमता है। इसके अलावा, वैश्विक और क्षेत्रीय जलवायु को विनियमित करने में इन पहाड़ों की महत्वपूर्ण भूमिका है। ग्लोबल वार्मिंग के कारण तेजी से बढ़ता तापमान इस क्षेत्र और अनुप्रवाहित क्षेत्र में रहने वाले लोगों के लिए विनाशकारी हो सकता है क्योंकि पहाड़ी हिमनद पानी और ऊर्जा की मांग को पूरा करने के लिए महत्वपूर्ण हैं, विशेषतः अनुप्रवाह क्षेत्र में। इसलिए, जलवायु में कोई भी परिवर्तन आजीविका पर व्यापक प्रभाव डाल सकता है क्योंकि वार्षिक जल सुरक्षा और खाद्य सुरक्षा पूर्ण रूप से इस क्षेत्र में बर्फ और हिमनद के पिघलने पर निर्भर है। हालांकि, अलग-अलग उप-क्षेत्रों में ग्लोबल वार्मिंग के अलग-अलग प्रभाव हो सकते हैं और, अलग-अलग परिणाम हो सकते हैं। इसलिए, जल उपलब्धता पर बदलती जलवायु के प्रभाव के अनुकूलन और प्रतिरोधक्षमता की योजना के लिए विश्वसनीय परिदृश्यों पर आधारित अनुमानों की आवश्यकता है।

उत्तर-पश्चिमी हिमालय में स्थित ब्यास बेसिन पर जल-जलवायु प्रतिरूपण, उनके अध्ययन में वर्तमान और भविष्य की जलवायु के तहत जल संचरण एवं वितरण के प्रतिरूपों का आकलन करने का प्रयास किया गया है। इस शोध प्रबंध का उद्देश्य वृहद् रूप से चार कार्यों में विभाजित है जो अध्ययन क्षेत्र में वर्षा अनुकरण की क्षमता का आकलन करने के लिए चयनित Microphysics और Cumulus मानकीकरण के लिए Weather Research and Forecasting (WRF) प्रतिरूपण के संवेदनशीलता विश्लेषण के साथ शुरू होता है। इसके बाद, वर्तमान और भविष्य की जलवायु के तहत अध्ययन क्षेत्र में हिमनद की गतिशीलता का आकलन करने के लिए हिमनद प्रतिरूपण का उपयोग किया गया था। इसके बाद, स्वचालित दृष्टिकोण का उपयोग करके WRF-Hydro को मापांकित किया गया। अंत में, WRF और WRF-Hydro की ऑफ़लाइन युग्मित प्रणाली का उपयोग वर्तमान और भविष्य की जलवायु के तहत जल-जलवायु संचरण एवं वितरण के प्रतिरूपों का आकलन करने के लिए किया गया था।

सबसे पहले, WRF को तीन अलग आकार के केंद्रित क्षेत्रों को डोमेन के साथ स्थापित किया गया था, सबसे बाहरी पूरे हिमालय को समाहित करता है, मध्य हिमालय के पूरे उत्तर-पश्चिम पर्वतमाला को समाहित करता है, और आंतरिक अध्ययन क्षेत्र में केंद्रित है। तीन Microphysics और दो Cumulus मानकीकरण के संयोजन के साथ छह प्रयोग किए गए। यह पाया गया कि हिमालय की तलहटी (बेसिन निर्गम के पास) के साथ वर्षा को छह में से चार प्रयोगों में कम करके आंका गया है। केवल WSM6_BMJ (WSM6 Microphysics और BMJ Cumulus मानकीकरण) और MP8_BMJ (MP8 Microphysics और BMJ Cumulus मानकीकरण) ही इन तलहटी में काफी मात्रा में वर्षा दिखाने में सक्षम थे। हालांकि, सभी छह प्रयोगों ने ऊर्ध्वप्रवाह क्षेत्र में और उत्तर-पश्चिमी हिमालय में पर्वत चोटियों और पर्वतमालाओं में उच्च वर्षा को दिखाया। दिसंबर-जनवरी-फरवरी (DJF) के दौरान, MP8_KF, MP3_BMJ, और

MP8_BMJ में अपेक्षाकृत कम वर्षा हुई है, हालांकि, WSM6_KF और WSM6_BMJ में अधिकतम वर्षा पाई गई। MP8_KF में कम से कम सामान्यीकृत मानक विचलन पाया गया है, साथ ही अधिकांश प्रयोगों की तुलना में उच्च कौशल प्रदर्शित करता है। कुल मिलाकर, MP8_KF को इसके कम विचलन और बेहतर कौशल के कारण उचित माना जा सकता है। जून-जुलाई-अगस्त-सितंबर (JJAS) के लिए, छह प्रयोगों में से चार (MP3_KF, MP3_BMJ, MP8_KF, WSM6_KF) बेसिन निर्गम और उत्तरी ढलानों पर अनुप्रवाहित तलहटी में वर्षा की विशेषताओं को दिखाने में विफल रहे, जिसमें औसत वर्षा बहुत कम थी। अवलोकन की तुलना में, WSM6_BMJ ने न्यूनतम सामान्यीकृत मानक विचलन के साथ-साथ उच्चतम सहसंबंध और सर्वोत्तम कौशल दिखाया है।

इसके बाद, हिमनद की गतिशीलता को वर्तमान (1980–2015) और भविष्य की जलवायु (2006–2100) के लिए RCP4.5 और RCP8.5 ग्लोबल वार्मिंग परिदृश्यों के तहत ब्यास बेसिन (उत्तर-पश्चिमी हिमालय में स्थित) पर अनुकरण और विश्लेषण किया गया था। Open Global Glacier Model (OGGM) को पहले अध्ययन क्षेत्र में मापांकित किया गया था और फिर वर्तमान (ERA-I forcing) और भविष्य (CMIP5 output forcing) जलवायु के लिए अनुकरण आयोजित किया गया था। वर्तमान जलवायु के लिए, प्रतिरूपण से पता चलता है कि कुल हिमनद मात्रा का 50% (1980 की तुलना में) 2011 तक खो गया है, हिमनद क्षेत्र और आयतन में हाल के दशकों के दौरान हिमनद क्षेत्र में उच्च उतार-चढ़ाव के साथ काफी घटती प्रवृत्ति दिखाई दे रही है। भविष्य के अनुमान RCP4.5 के तहत 2040 ± 2.5 वर्ष तक 75% हानि और 2094 ± 3.5 वर्षों तक ~90% हानि का सुझाव देते हैं। RCP8.5 के तहत, 2040 ± 3 साल तक 75% नुकसान और 2084 ± 8 साल तक 90% नुकसान होने की उम्मीद है। निकट-सतह के वायु तापमान (मासिक माध्य और वार्षिक माध्य दोनों) माध्य संपूर्ण 21वीं सदी के लिए RCP4.5 और RCP8.5 के तहत उल्लेखनीय रूप से बढ़ती प्रवृत्ति को दर्शाता है। कुल मासिक वर्षा RCP4.5 के तहत कोई प्रवृत्ति नहीं दिखाता है, हालांकि, यह ODJFMA महीनों के लिए घटती प्रवृत्ति और RCP8.5 के तहत JJ महीनों के लिए बढ़ती प्रवृत्ति को दर्शाता है। JJ वर्षा में वृद्धि हिमनद द्रव्यमान में वृद्धि नहीं करती है क्योंकि इस क्षेत्र में इन महीनों के दौरान बर्फबारी नहीं होती है। RCP4.5 के तहत, NDJF के दौरान बर्फबारी कोई महत्वपूर्ण प्रवृत्ति नहीं दिखाती है, हालांकि, यह अक्टूबर और मार्च के दौरान घटती प्रवृत्ति को दर्शाता है। RCP8.5 के तहत, अक्टूबर से मार्च तक बर्फबारी एक महत्वपूर्ण गिरावट की प्रवृत्ति दर्शाती है। कुल मिलाकर, एक समान पिघलने की दर RCP4.5 और RCP8.5 के तहत ~ 2050 तक पाई गई, लेकिन बाद में उच्च दर दिखाई देती है।

इसके बाद, WRF-Hydro मापांकन, WRF कम पैमाने पर उद्धृत मौसम जानकारी का उपयोग करके किया गया था। मॉडल को 2003 के लिए मापांकित किया गया था और 2004-2005 के लिए सत्यापित किया गया था। बेसिन निर्गम पर स्टेशन ने देखा कि प्रवाह का उपयोग मापांकन और सत्यापन करने के लिए किया गया था। प्रतिरूपण के विरूपण प्रक्रिया के माध्यम से PEST (Parameter Estimation) उपकरण का उपयोग करके चयनित 42 मापदंडों को संशोधित किया गया था। आठ अनुकरण मौसमी जानकारी के दो समूहों (MP8KF मौसमी जानकारी और WSM6BMJ मौसमी जानकारी) का उपयोग करके नियत किए गए थे। यह पाया गया है कि मॉडल मापांकन ने बेसिन प्रवाह

को पुनः उत्पन्न करने के लिए सटीकता में सुधार किया। सुधार के बावजूद, MP8KF प्रयोगों में JJAS निर्वहन को कम करके आंका गया था, संभवतः MP8KF की मौसमी जानकारी में JJAS वर्षा को कम करके आंका गया था। WSM6BMJ प्रयोगों ने JJAS के लिए काफी अच्छा प्रदर्शन किया, लेकिन इसने गैर-JJAS के लिए कुछ गलत अधिकतम प्रवाह को दिखाया। यह गलत प्रवाह संभवतः WSM6BMJ मौसमी जानकारी में वर्षा (गैर-JJAS के लिए) की अधिकता के कारण उद्धृत हुए थे। इसके अलावा, MP8KF और WSM6BMJ प्रयोग के समूहों में से सर्वश्रेष्ठ प्रयोग को चुना गया था। फिर, इन सर्वश्रेष्ठ उम्मीदवारों से बेसिन प्रवाह के Ensemble Mean और Weighted Ensemble Mean की गणना की गई। मापांकित (NSE = 0.64) प्रवाह के लिए Ensemble Mean यथोचित रूप से अच्छी तरह से पाया गया था, हालांकि, सत्यापन अवधि के लिए सटीकता कम हो जाती है। हालांकि, सत्यापन अवधि (NSE = 0.6) के लिए Weighted Ensemble Mean सटीकता बढ़ाने के साथ-साथ संतोषजनक परिणाम (NSE = 0.5) उत्पन्न करता है।

इसके बाद, WRF-Hydro के साथ WRF को ऑफलाइन जोड़ा गया। उच्च-रिज़ॉल्यूशन मौसमी जानकारी (एक ऐतिहासिक समयावधि एवं RCP4.5 और RCP8.5 के तहत भविष्य के अनुमानों के लिए तीन समयावधि) के लिए WRF प्रतिरूपण का उपयोग करके अनुकरण का प्रदर्शन किया गया था। इन मौसमी जानकारी को उच्च-रिज़ॉल्यूशन जल एवं जलवायु के संचरण एवं प्रतिरूपों के प्रकार उत्पन्न करने के लिए जल प्रतिरूपण (WRF-Hydro) को निविष्ट किया गया था। अद्यतन हिमनद सीमाएँ, हिमनद प्रतिरूपण से प्राप्त की गईं और बाद में एक अद्यतन भूमि उपयोग भूमि कवर (LULC) का प्रतिनिधित्व करने के लिए WRF और WRF-Hydro में निविष्ट किया गया। यह पाया गया कि बेसिन पर वर्षा की कुल मात्रा बेसिन में नहीं बदलती है, हालांकि, वर्षा स्वरूप के परिवर्तन में एक महत्वपूर्ण विपरीतता है। बेसिन की ऊंची चोटियों पर RCP4.5 और RCP8.5 दोनों के तहत कम वर्षा का अनुभव होने की उम्मीद है, जो RCP8.5 के तहत 21वीं सदी के अंत में सबसे बड़ी गिरावट है। इसके विपरीत, अनुप्रवाहित क्षेत्र ऐतिहासिक समय अवधि की तुलना में अधिक वर्षा प्राप्त कर सकता है। इसके विपरीत ज्यादातर विभिन्न मौसमों (DJF और JJAS) के दौरान अलग-अलग प्रतिक्रियाओं के संयोजन के कारण पाया गया। RCP 4.5 और RCP 8.5 परिदृश्यों के तहत पूरे वार्षिक चक्र में सतह के पास हवा का तापमान बढ़ने की उम्मीद है। हालांकि RCP4.5 2050 के बाद स्थिर हो जाता है, RCP8.5 में वृद्धि जारी है, जिससे 2050 के बाद इन दोनों परिदृश्यों के तापमान के बीच महत्वपूर्ण अंतर होता है। 21वीं सदी के अंत में अध्ययन क्षेत्र के RCP4.5 के तहत 1-3 डिग्री सेल्सियस और JJAS के लिए RCP8.5 के तहत 3-4 डिग्री सेल्सियस गर्म होने की उम्मीद है। इस सदी के अंत में DJF के RCP4.5 के तहत 2.5-3.5 डिग्री सेल्सियस और RCP8.5 के तहत 4.5-5 डिग्री सेल्सियस तक गर्म होने की उम्मीद है। सतही अपवाह के लगभग पूरे बेसिन में घटने की संभावना है। हालाँकि, यह RCP4.5 के तहत 21वीं सदी की शुरुआत में और RCP8.5 के तहत 21वीं सदी के मध्य में ऊंची चोटियों पर बढ़ा हुआ पाया गया। सबसे अधिक गिरावट इस सदी के अंत में RCP4.5 और RCP8.5 दोनों के तहत उच्च ऊंचाई वाले क्षेत्रों में पाई गई। उपसतह प्रवाह (UGDRNOFF) RCP4.5 और RCP8.5 दोनों के तहत लगातार कम होता गया, हालाँकि RCP8.5 के तहत एक मजबूत गिरावट के संकेत देखे गए। इस सदी के अंत में UGDRNOFF के RCP4.5 के तहत ~60% और RCP8.5 के तहत

~70% की कमी होने की उम्मीद है। RCP4.5 के तहत, 5 किमी से कम ऊंचाई वाले क्षेत्रों के लिए बर्फ के पानी के समतुल्य (SNEQV) में कमी पाई गई, हालांकि, उच्च ऊंचाई वाले क्षेत्रों के लिए इसे बढ़ा हुआ पाया गया। 21 वीं सदी के मध्य तक RCP8.5 के तहत इसी तरह की प्रतिक्रिया की उम्मीद है, हालांकि, सदी के अंत तक, SNEQV के पूरे क्षेत्र में पूरे वर्ष घटने की उम्मीद है। SNEQV में सबसे ज्यादा गिरावट 21वीं सदी के अंत में RCP4.5 और RCP8.5 दोनों परिदृश्यों में हो सकती है। इस सदी के अंत में दोनों परिदृश्यों में SNEQV की विपरीत प्रतिक्रिया वार्मिंग के विभिन्न स्तरों के कारण हो सकती है।

Table of Contents

Certificate	i
Acknowledgment.....	ii
Abstract.....	iii
सारांश	vi
Table of Contents	x
List of Figures.....	xiv
List of Tables.....	xx
List of Acronyms	xxii
1 Introduction.....	1
1.1 Introduction	1
1.1.1 Context: Freshwater potential and availability	1
1.2 Hydrology, Land, and Atmosphere	1
1.3 Hydroclimate Processes	2
1.4 Climate Change	2
1.4.1 Himalayas and Climate Change	3
1.4.1.1 Western Himalayas	3
1.4.2 Glaciers' status and water availability	4
1.5 Global versus regional studies.....	5
1.6 Climate Change Scenarios	6
1.7 Downscaling.....	7
1.7.1 Weather Research and Forecasting (WRF)	8
1.8 Hydrological modeling.....	9
1.8.1 Model Calibration.....	10
1.9 Glacier modeling	11
1.10 Parameter ESTimation (PEST) Tool.....	12
1.11 Study Region	13
1.12 Research problems and objectives	14

2 Sensitivity of Precipitation Simulation over Beas Basin to Microphysics and Cumulus Parameterizations in WRF.....	16
2.1 Introduction.....	16
2.2 Data and Methods.....	19
2.2.1 Model Configuration and setup.....	19
2.2.2 Microphysics Schemes.....	21
2.2.3 Cumulus Schemes.....	21
2.2.4 Observation Datasets.....	22
2.3 Results.....	22
2.3.1 Observation Precipitation Data.....	22
2.3.2 Cumulus and Microphysics Sensitivity.....	26
i. Annual precipitation.....	26
ii. DJF Precipitation.....	27
iii. JJAS Precipitation.....	28
2.3.3 Accuracy and Goodness of fit (GoF).....	29
2.4 Summary and Discussion.....	33
2.4.1 Cumulus Parameterization.....	33
2.4.2 Microphysics.....	37
3 Glacial Changes over Beas Basin under Present and Future Climates	43
3.1 Introduction.....	43
3.2 Data and Methods.....	45
3.2.1 Model Description.....	45
3.2.2 Model Setup and Data Used.....	48
3.2.3 Model Calibration.....	49
3.2.4 Model Simulation for RCP Projections.....	50
3.3 Results.....	51
3.3.1 Model Performance.....	51
3.3.2 Observed Changes in Glacier Area and Volume in Present Climate.....	53
3.3.3 Projected Changes in Glacier Area and Volume under Global Warming for 21 st Century.....	55

i. RCP4.5	55
ii. RCP8.5	58
3.4 Summary and Discussion	60
4 WRF-Hydro Calibration and its Parameter Sensitivity	61
4.1 Introduction	61
4.1.1 Regularisation	62
4.2 Data and Methods	63
4.2.1 WPS pre-processing	63
4.2.2 WRF setup and configuration	64
4.2.3 WRF-Hydro setup and configuration	65
4.2.4 The design of experiments	67
4.2.4.1 One-At-a-Time (OAT) Sensitivity	69
4.2.4.2 Calibration under PEST	70
4.3 Results	73
4.3.1 Parameter Identifiability	73
4.3.2 Calibration and Validation	74
i. MP8KF Experiments	74
ii. WSM6BMJ Experiments	75
iii. WSM6BMJ (JJAS) Experiments	77
iv. MP8WSM Experiments	78
4.3.3 Calibration constrained Parameter variation and sensitivity	81
4.4 Summary and Discussion	85
5 Future Water Availability over Beas Basin	90
5.1 Introduction	90
5.2 Data and Methods	92
5.2.1 Glacier Modelling	93
5.2.2 WPS pre-processing	94
5.2.3 WRF setup and configuration	94
5.2.4 WRF-Hydro setup and configuration	96
5.2.5 Ensemble of WRF-Hydro fluxes	98

5.3 Results.....	99
5.3.1 Glacier Boundaries	99
5.3.2 Meteorological Forcing	101
i. Precipitation (ANN).....	101
ii. Precipitation (DJF).....	103
iii. Precipitation (JJAS)	104
iv. Near-surface air temperature.....	105
5.3.3 Hydrological Fluxes	107
i. Surface Runoff	107
ii. Underground/Subsurface Runoff.....	108
iii. Snowmelt runoff	109
iv. Snow water equivalent.....	110
v. Basin Discharge.....	112
5.4 Summary and Discussion.....	116
6 Conclusion and Future Work.....	119
6.1 Conclusion.....	119
6.2 Future work.....	122
Publications and Conferences.....	123
References.....	124
Appendix A1	142
Appendix A2	149
Appendix A3	151
Biographical Sketch	153

List of Figures

Figure 1. 1 – The mountain ranges of the Himalayas	4
Figure 1. 2 – Schematic diagrams of the WRF-Hydro coupler and components. From the technical description of WRF-Hydro (Adopted from Gochis et al. 2018).	9
Figure 1. 3 – Schematic diagram of glacier flowline as adopted in OGGM model.	11
Figure 1. 4 - Beas basin with basin boundary, underlaid by Digital Elevation Model (SRTM 90 m). The highest and lowest elevations within the basin boundary are approximately 6545 masl and 826 masl. The sky blue region represents the glaciers in the domain. Glaciers in this region cover approximately 12.6% of the total area.	14
Figure 2. 1 - Three-level nested WRF domain used in this study. Outer domain (d01) has a horizontal resolution of 25 km with 165 grids in the south-north direction and 184 grids in the west-east direction. The intermediate domain (d02) has a horizontal resolution of 10 km, with 153 grids in the south-north direction and 174 grids in the west-east direction. The inner domain (d03) has a horizontal resolution of 3 km, with 75 grids in the south-north direction and 72 grids in the west-east direction.	20
Figure 2. 2- Total Annual precipitation (for domain d03) during 2003 for (a) IMD, (b) APHRODITE, (c) TRMM, (d) PERSIANN-CDR, (e) CPC, (f) CHIRPS, (g) CRU and (h) GPCP.....	23
Figure 2. 3 - Quantile-Quantile plot (Q-Q plot) between gridded observations (TRMM, APHRODITE, CHIRPS, CPC, GPCP, IMD, and PERSIANN) and in-situ observations at locations Banjar, Bhuntar, Janjheli, Larji, Manali, Pandoh, and Sainj. The blue dots are quantile to quantile plot, whereas green dots are scatter plot. Red line is the regression line corresponding to the quantile-quantile plot. Black line is the reference line.....	25
Figure 2. 4 - (a) Annual mean observed precipitation from APHRODITE. WRF simulated annual mean precipitation over d03 during 2003: (b) WSM6_KF, (c) MP3_KF, (d) MP8_KF, (e) WSM6_BMJ, (f) MP3_BMJ, and (g) MP8_BMJ. The red color numbers at the right top corner is the areal-temporal average precipitation in mm/day.....	26
Figure 2. 5 - Quantile Quantile plot (Q-Q plot) between WRF simulated precipitation and Aphrodite for 2003. The WRF simulated experiments (WSM6_KF, WSM6_BMJ, MP8_KF, MP8_BMJ, MP3_KF, and MP3_BMJ) are plotted against Aphrodite precipitation for ANN (a), DJF (b), and JJAS (c). The blue dots are quantile to quantile plot, whereas green dots are scatter plot. Red line is the regression line corresponding to the quantile-quantile plot. Black line is the reference line.....	28
Figure 2. 6 - Taylor plots using spatial (a,c, and e) and temporal correlation (b, d, and f) between WRF experiments (WSM6_KF, WSM6_BMJ, MP8_KF, MP8_BMJ, MP3_KF, and MP3_BMJ) and APHRODITE precipitation for 2003. Taylor plots are showing correlation, normalized standard deviation, and contours as skill score for ANN (a and b), DJF (c and d), and JJAS (e and f).	32

Figure 2. 7 - The maximum available CAPE for each grid point over d02, overlapping with d03, for MP8_BMJ, MP8_KF, WSM6_BMJ, and WSM6_KF (a-d). (a) shows maximum CAPE over all vertical levels, for each gridpoint and timesteps. (b) shows CDF for the values shown in (a). (c) shows maximum CAPE at 550 hPa vertical level for each grid point and timesteps. (d) shows CDF for the values shown in (c). (e) shows LFC and (f) shows LFL over each grid point and each timestep for these experiments34

Figure 2. 8 - The areal and temporal averaged U (b and e), V (c and f), and W (a and d) wind components varying with vertical levels. These averaged wind components over vertical levels are shown for WRF eperiments; MP8_BMJ, MP8_KF, WSM6_BMJ, and WSM6_KF36

Figure 2. 9 - The JJAS-averaged vertical cross section of QVAPOR mixing ratio for d02 at d03 boundaries. Gray shaded area shows mountains. (a-d) shows actual average mixing ratio for WSM6_BMJ at east (a), west (b), north (c), and south (d) boundaries. Further, mixing ratio is shown for MP8_BMJ – WSM6_BMJ (e-h), MP8_KF – WSM6_BMJ (i-l), and WSM6_KF – WSM6_BMJ (m-p) for vertical cross section of east (e, i, and m), west (f, j, and n), north (g, k, and o), and south (h, l, and p) boundaries.38

Figure 2. 10 - The JJAS-averaged vertical cross section of relative humidity for d02 at d03 boundaries. Gray shaded area shows mountains. (a-d) shows actual average mixing ratio for WSM6_BMJ at east (a), west (b), north (c), and south (d) boundaries. Further, mixing ratio is shown for MP8_BMJ – WSM6_BMJ (e-h), MP8_KF – WSM6_BMJ (i-l), and WSM6_KF – WSM6_BMJ (m-p) for vertical cross section of east (e, i, and m), west (f, j, and n), north (g, k, and o), and south (h, l, and p) boundaries.39

Figure 2. 11 - Area-averaged mixing ratio (dbz, QVAPOR, QRAIN, QICE, QGRAUP, and QCLOUD) over d03. Mixing ratios are shown as they varying over model levels with time for MP8_KF, MP8_BMJ, WSM6_KF, and WSM6_BMJ. The unit of mixing ratio is g/kg.41

Figure 3. 1- Computed centrelines for Glacier RGI60-14.1534046

Figure 3. 2- Catchment area for centrelines of Glacier RGI60-14.1534046

Figure 3. 3- Computed geometrical widths of Glacier RGI60-14.1534047

Figure 3. 4- Corrected geometrical widths of Glacier RGI60-14.1534047

Figure 3. 5- (a) shows the FCC image of the LANDSAT-3 L1TP product, acquired on 04 October 1980. The image is classified through supervised learning using (b) Maximum Likelihood (~0.97 accuracy), (c) Support Vector Machine (~ 0.98 accuracy), and (d) Random Tree algorithms (~0.96 accuracy) methods. The main interest was to classify the area of glacier cover.....53

Figure 3. 6- Glacier dynamics in Beas basin, in terms of their volume and extent area during 1980-2015: (a) total glacier volume, (b) total glacier area, (c) change in volume of each glacier entity (447 glacier entities) for few representative years, and (d) change in the area of each glacier entity for few representative years.54

Figure 3. 7- Glacier thickness in Beas basin with flowlines using OGGM forced by meteorological data obtained from the EC-EARTH model (from CMIP5). The projected glacier thickness is shown for three representative periods (2025, 2055, 2085) under RCP4.5 (a-c) and RCP8.5 (d-f).....55

Figure 3. 8 - Glacier volume using OGGM with meteorological forcing from selected CMIP5 models: (a) RCP4.5, and (b) RCP8.5. The green, yellow and red spans represent the projected timeline for 50%, 75%, and 90% loss, respectively. These spans represent the range of the timeline suggested by multi CMIP5 models. The red dotted line in (b) shows the starting point of the 90% loss uncertainty under RCP4.5 (shown in a). Arrow to the left of a red dotted line refers to 90% loss uncertainty advancement under the RCP8.5 scenario. (c) the projected loss of glacier volume for individual models is shown for 2050, 2075, and 2099 under RCP4.5 and RCP8.5. (d) the projected timeline for 50%, 75% and 90% loss for individual models under RCP4.5 and RCP8.5. The green, yellow, and red lines (in c) show the mean glacial loss for 2050, 2075, and 2099, dotted line with points for RCP4.5 and dotted line for RCP8.5. The green, yellow, and red lines (in d) shows the mean year corresponding to the 50%, 75% and 90% loss, dotted line with points for RCP4.5 and dotted line for RCP8.5. Black dotted line in (d) shows the 50% loss corresponding to the historical starting point. Magenta color in (c-d) represents the location of CESM1-CAM5.....57

Figure 3. 9 - The ensemble mean monthly precipitation (a) and temperature (b) are shown for the glaciers' location under RCP4.5 and RCP8.5 projections (95% CI). (c) shows the amount of solid precipitation out of total precipitation, which is shown in (a).58

Figure 3. 10 - Ensemble mean time series of precipitation (a, b, c) and temperature (d, e, f) for DJF (a, d), JJA (b, e), and Annual (c, f) under RCP4.5 and RCP8.5.....59

Figure 4. 1 – The glacier representation in the MODIS LULC, blue color in b-d represents the glacier. (a) shows the zoomed high-resolution satellite image over the Bada Shigri glacier, overlaid by the RGI V6 glacier boundary. The debris over the glacier makes it difficult to distinguish between the classes glacier and barren rock. (b) shows the default MODIS LULC. (c) shows the MODIS LULC overlaid with RGI V6 glacier boundaries in the region. (d) shows the updated MODIS LULC with corrected glacier boundaries64

Figure 4. 2 – The flowchart of the WRF-Hydro calibration experiments.68

Figure 4. 3 – The schematic diagram represents the parallel processing during the model (WRF-Hydro) inversion (model calibration) under the PEST framework.68

Figure 4. 4– The parameter identifiability plot of all 42 parameters, using 25, 30, 36, and 42 singular values. (a) shows PI using the MP8KF forcing, (b) shows PI using the WSM6BMJ forcing.....73

Figure 4. 5 – Comparison of PEST-calibrated/validated discharge (with MP8KF forcing) through estimation and regularisation mode with default model discharge and observed discharge at the basin outlet. Top x-axis and right y-axis show precipitation from APHRODITE and WRF simulation (MP8KF forcing)74

Figure 4. 6– Comparison of PEST-calibrated/validated discharge (with WSM6BMJ forcing) through estimation and regularisation mode with default model discharge and observed discharge at the basin outlet. Top x-axis and right y-axis show precipitation from APHRODITE and WRF simulation (WSM6BMJ forcing).....76

Figure 4. 7– Comparison of PEST-calibrated/validated discharge (with WSM6BMJ forcing for JJAS only) through estimation and regularisation mode with default model discharge and observed discharge at the basin outlet. Top x-axis and right y-axis show precipitation for APHRODITE and WRF simulation (WSM6_BMJ forcing).....77

Figure 4. 8– Comparison of ensemble of PEST-calibrated/validated discharge (with MP8KF and WSM6BMJ forcing) through estimation and regularisation mode with default model discharge and observed discharge at basin outlet.80

Figure 4. 9– The variations in the parameter value of all adjustable parameters used in the inversion process with MP8KF forcing. The parameter variations are shown over the optimization iterations during the calibration process in regularisation mode with SVD and LSQR inverse solutions. The solid line shows the parameter variations, and the dashed line shows the parameter value in the most optimized iteration. The green color represents SVD regularisation, and yellow represents LSQR regularisation.83

Figure 4. 10– The variations in the parameter sensitivity of all adjustable parameters used in the inversion process with MP8KF forcing. The composite parameter sensitivity is shown over the optimization iterations during the calibration process in regularisation mode with SVD and LSQR inverse solution. The solid line shows the parameter sensitivity, and the dashed line shows the parameter sensitivity in the most optimized iteration. The green color represents SVD regularisation, and yellow represents LSQR regularisation.84

Figure 4. 11– The area-averaged daily precipitation for year 2003 simulated through WRF with MP8KF and WSM6BMJ parameterizations along with observation from APHRODITE.86

Figure 5. 1 – The flow chart of offline coupled setup of the WRF, WRF-Hydro and OGGM model to produce the hydroclimate projections.93

Figure 5. 2 – The projected glacier boundaries for the future representative years of the 21st century under the RCP4.5 (a-c) and RCP8.5 (d-f) scenarios. The representative years are 2025 (a,d) for early 21st century, 2050 (b,e) for mid 21st century, and 2085 (c, f) for end 21st century. (g) shows the loss of glacier area for these years with respect to the start of the 21st century..... 100

Figure 5. 3 – The annual average daily precipitation for the (a) historical period (1995-2005). The contours show standard deviation. The difference of annual average daily precipitation between historical time slice and future representative time slices for (b,e) early-21st-century (2025-2035), (c,f) mid-21st-century (2050-2060), and (d,g) end-21st-century (2085-2095) under (b,c,d) RCP4.5 and (e,f,g) RCP8.5 scenarios are shown. The hatching shows the significant changes computed through two times sigma on the bootstrapped mean and standard deviation..... 101

Figure 5. 4 – The DJF average daily precipitation for the (a) historical period (1995-2005). The contours show the standard deviation. The difference of DJF average daily precipitation between historical time slice and future representative time slices for (b,e) early-21st century (2025-2035), (c,f) mid-21st century (2050-2060), and (d,g) end-21st century (2085-2095) under (b,c,d) RCP4.5 and (e,f,g) RCP8.5 scenarios are shown. The hatching shows the significant changes computed through two times sigma on the bootstrapped mean and standard deviation..... 103

Figure 5. 5 – The JJAS average daily precipitation for the (a) historical period (1995-2005). The contours show the standard deviation. The difference of JJAS average daily precipitation between historical time slice and future representative time slices for (b,e) early-21st century (2025-2035), (c,f) mid-21st century (2050-2060), and (d,g) end-21st century (2085-2095) under (b,c,d) RCP4.5 and (e,f,g) RCP8.5 scenarios are shown. The hatching shows the

significant changes computed through two times sigma on the bootstrapped mean and standard deviation.....	104
Figure 5. 6 – The basin area-averaged daily air temperature for all months of a year under historical, RCP4.5, and RCP8.5 scenarios. The time slice of 11 years was taken to represent historical and future climates. A total of three slices were taken to represent the early, mid, and end of the 21st century.....	105
Figure 5. 7 – The basin averaged daily mean of near surface air temperature for (a) historical period (1995-2005). The dotted line shows the average near surface temperature for JJAS (black dotted line) and DJF (red dotted line). The difference of basin averaged daily mean of near surface air temperature between historical time slice and future representative time slices for (b,e) early-21st-century (2025-2035), (c,f) mid-21st-century (2050-2060), and (d,g) end-21st-century (2085-2095) under (b,c,d) RCP4.5 and (e,f,g) RCP8.5 scenarios are shown. The black and red dotted lines in panels b-g show the warming over the respective time period and scenarios for JJAS and DJF respectively.....	106
Figure 5. 8 – The annual average daily surface runoff in mm for the (a) historical period (1995-2005). The contours show standard deviation. The difference of annual average daily surface runoff between historical time slice and future representative time slices for (b,e) early-21st-century (2025-2035), (c,f) mid-21st-century (2050-2060), and (d,g) end-21st-century (2085-2095) under (b,c,d) RCP4.5 and (e,f,g) RCP8.5 scenarios are shown. The hatching shows the significant changes computed through 2σ on the bootstrapped mean and standard deviation.....	107
Figure 5. 9 – The annual average daily sub-surface runoff in mm for the (a) historical period (1995-2005). The contours show the standard deviation. The difference of annual average daily sub-surface runoff between historical time slice and future representative time slices for (b,e) early-21st-century (2025-2035), (c,f) mid-21st-century (2050-2060), and (d,g) end-21st-century (2085-2095) under (b,c,d) RCP4.5 and (e,f,g) RCP8.5 scenarios are shown. The hatching shows the significant changes computed through 2σ on the bootstrapped mean and standard deviation.....	108
Figure 5. 10 – The annual average daily snowmelt runoff in mm for the (a) historical period (1995-2005). The contours show the standard deviation. The difference of annual average daily snowmelt runoff between historical time slice and future representative time slices for (b,e) early-21st-century (2025-2035), (c,f) mid-21st-century (2050-2060), and (d,g) end-21st-century (2085-2095) under (b,c,d) RCP4.5 and (e,f,g) RCP8.5 scenarios are shown. The hatching shows the significant changes computed through 2σ on the bootstrapped mean and standard deviation.....	109
Figure 5. 11 – The basin averaged daily mean of snow water equivalent for (a) historical period (1995-2005). The dotted line shows the average near-surface temperature for JJAS (black dotted line) and DJF (red dotted line). The difference of basin averaged daily mean of snow water equivalent between historical time slice and future representative time slices for (b,e) early-21st-century (2025-2035), (c,f) mid-21st-century (2050-2060), and (d,g) end-21st-century (2085-2095) under (b,c,d) RCP4.5 and (e,f,g) RCP8.5 scenarios are shown. The black and red dotted lines in panels b-g show the warming over the respective time period and scenarios for JJAS and DJF respectively.....	110
Figure 5. 12 – The ANN average of ratio of precipitation and snowfall rate for the (a) historical period (1995-2005). The difference of ANN average of ratio of precipitation and snowfall rate between historical time slice and future representative time slices for (b,e) early-21st-century	

(2025-2035), (c,f) mid-21st-century (2050-2060), and (d,g) end-21st-century (2085-2095) under (b,c,d) RCP4.5 and (e,f,g) RCP8.5 scenarios are shown. 112

Figure 5. 13 – The daily discharge of Beas basin at Thalout for historical period (1995-2005), a representative of present climate, and future representative time slices for early-21st century (2025-2035), mid-21st century (2050-2060), and end-21st century (2085-2095) under RCP4.5 and RCP8.5 scenarios. The figure does not show fliers. 113

Figure 5. 14 - The probability of exceedence for daily discharge of Beas basin at Thalout for historical period (1995-2005), a representative of present climate, and future representative time slices for early-21st-century (2025-2035), mid-21st-century (2050-2060), and end-21st-century (2085-2095) under (a) RCP4.5 and (b) RCP8.5 scenarios. The exceedence probability was computed on the 95 percentile of discharge values..... 114

Figure 5. 15 - The wavelet power spectrum of daily discharge of Beas basin at Thalout for present climate represented by historical time slice (1995-2005) and future climate represented by time slices for (b,e) early-21st-century (2025-2035), (c,f) mid-21st-century (2050-2060), and (d,g) end-21st-century (2085-2095) under (b,c,d) RCP4.5 and (e,f,g) RCP8.5 scenarios. The dotted black line in a-g shows the 95% significance level. (i), (ii), and (iii) show the global scaled spectrum for the representative time slices of present climate, future climate under RCP4.5, and future climate under RCP8.5 respectively. The vertical lines in i-iii show the maximum scaled global power for the representative time slices of present climate and future climates (RCP4.5 and RCP8.5)..... 115

List of Tables

Table 1. 1 – The RCP scenarios and their associated level of warming and change in radiative forcing.....	7
Table 2. 1- List of WRF options used in this study	20
Table 2. 2 - List of observation datasets used in this study for observation intercomparison ..	22
Table 2. 3 - Performance metrics for ANN of the simulations with observation	32
Table 2. 4 - Performance metrics for DJF of the simulations with observation	32
Table 2. 5 - Performance metrics for JJAS of the simulations with observation.....	32
Table 3. 1– Total glacier volume in km ³ during different years. The volume is the ensemble mean of the glacier model output forced by CMIP5 model outputs, and uncertainty is represented through their standard deviation.....	56
Table 4. 1 – The selected options for the physical processes in the Noah-MP multiphysics parameterization.....	66
Table 4. 2 – The selected sensitive parameters after one-at-a-time sensitivity analysis. The violet color represents channel parameters, yellow represents soil parameters, green represents biophysical parameters, and cyan represents snow parameters.	69
Table 4. 3 – A list of experiments for the WRF-Hydro calibration under the PEST framework. The experiments include the traditional as well as more sophisticated (SVD or LSQR regularisation) numerical solutions to the inverse problem. The comment column shows the number of model years required to achieve the optimum solution.....	72
Table 4. 4 – The accuracy metrics of calibrated/validated WRF-Hydro discharge (using MP8KF forcing) with observed discharge. The metrics were calculated separately for calibration (2003) and validation period (2004-2005). d: index of agreement; KGE: Kling-Gupta Efficiency; NSE: Nash-Sutcliffe efficiency coefficient; RMSE: Root mean squared error.....	75
Table 4. 5 – The accuracy metrics of calibrated/validated WRF-Hydro discharge (using WSM6BMJ forcing) with observed discharge. The metrics were calculated separately for calibration (2003) and validation period (2004-2005). d: index of agreement; KGE: Kling-Gupta Efficiency; NSE: Nash-Sutcliffe efficiency coefficient; RMSE: Root mean squared error.....	76
Table 4. 6 – The accuracy metrics of calibrated/validated WRF-Hydro discharge (using WSM6BMJ forcing for JJAS only) with observed discharge. The metrics were calculated	

separately for calibration (2003) and validation period (2004-2005). d: index of agreement; KGE: Kling-Gupta Efficiency; NSE: Nash-Sutcliffe efficiency coefficient; RMSE: Root mean squared error. 78

Table 4. 7 – The accuracy metrics of an ensemble of calibrated/validated WRF-Hydro discharge (using MP8KF and WSM6BMJ forcing) with observed discharge. The metrics were calculated separately for calibration (2003) and validation period (2004-2005). d: index of agreement; KGE: Kling-Gupta Efficiency; NSE: Nash-Sutcliffe efficiency coefficient; RMSE: Root mean squared error. 80

Table 5. 1– The description of the glacier simulations using the OGGM model. 94

Table 5. 2 – The list of experiments for WRF simulations. The representative climate, projected scenario, representative time period, source of IC/BC, and parameterizations are listed. 96

Table 5. 3 – The list of experiments for hydrological simulations using WRF-Hydro. The representative climate, projected scenario, representative time period, source of IC/BC and calibrated version of WRF-Hydro are listed. 98

Table 5. 4 – The ensemble meteorological/hydrological fluxes for the present and future climates representatives. The representative climate, projected scenario, representative time period, and ensemble calculation method are listed. 99

List of Acronyms

ACSNOM	Snowmelt
AGGFACTRT	Aggregation Factor
ANN	Annual Cycle
APHRODITE	Asian Precipitation – Highly-Resolved Observational Data Integration Towards Evaluation
AR	Assessment Report
BMJ	Betts–Miller–Janjić
CAM	Community Atmosphere Model
CAPE	Convective Available Potential Energy
CDF	Cumulative Density Function
CESM	Community Earth System Model
CFSR	Climate Forecast System Reanalysis
CHIRPS	Climate Hazards Group InfraRed Precipitation with Station data
CI	Confidence Interval
CMIP5	Coupled Model Intercomparison Project Phase 5
CPC	Climate Prediction Center
CRU	Climate Research Unit
d	index of agreement
dbz	simulated radar reflectivity
DEM	Digital Elevation Model
DJF	December-January-February
DN	Digital Number
ECMWF	European Centre for Medium-Range Weather Forecasts
ELA	Equilibrium Line Altitude
ERA-I	ECMWF Reanalysis - Interim
GCM	General Circulation Model
GD	Grell-Devenyi
GHG	Greenhouse Gas
GIS	Geographic Information System
GLIMS	Global land Ice Measurement from Space Initiatives
GLOF	Glacier Lake Outburst Flood

GPCP	Global Precipitation Climatology Project
IGP	Indo-Gangetic Plains
IMD	India Meteorological Department
IPCC	Intergovernmental Panel on Climate Change
ISM	Indian Summer Monsoon
ISRO	Indian Space Research Organisation
JJAS	June-July-August-September
KF	Kain-Fritsch
KGE	Kling Gupta Efficiency coefficient
LCL	Lifted Condensation Level
LFC	Level of Free Convection
LSQR	Least Square
LULC	Land Use Land Cover
ME	Mean Error
MODIS	Moderate Resolution Imaging Spectroradiometer
MP	Microphysics Parameterization
NCAR	National Center for Atmospheric Research
NSE	Nash-Sutcliffe Efficiency
OGGM	Open Global Glacier Model
PERSIANN-CDR	Precipitation Estimation from Remotely Sensed Information using Artificial Neural Networks- Climate Data Record
PEST	Parameter Estimation Tool
PHIRATSUF	phi ratio sufficient
PHIREDLM	phi reduced lambda
PHIRESTP	phi reduced stop
PHIREDSWH	phi reduced switch
PI	Parameter Identifiability
Q₁₀	high flows
Q₅₀	median flow
Q₉₀	low flows
QCLOUD	cloud water mixing ratio
QGRAUP	graupel mixing ratio
QICE	ice mixing ratio
Q-Q plot	Quantile-Quantile plot

QRAIN	rainwater mixing ratio
QSNOW	snow mixing ratio
QVAPOR	Water vapor mixing ratio
R	Correlation coefficient
RCM / LAM	Regional Climate Model / Limited Area Model
RCP	Representative Concentration Pathway
RGI	Randolph Glacier Inventory
rh	relative humidity
RMSE	Root Mean Square Error
SFCRNOFF	Surface Runoff
SNEQV	snow water equivalent
SRTM	Shuttle Radar Topography Mission
SVD	Singular Value Decomposition
TOA	Top of Atmosphere
TP	Tibetan Plateau
TRMM	Tropical Rainfall Measuring Mission
UGDRNOFF	Subsurface Runoff / Underground Runoff
USGS	United States Geological Survey
WD	Western Disturbance
WPS	WRF Pre-processing System
WRF	Weather Research and Forecasting
WSM	WRF single moment